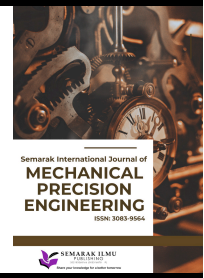




Semarak International Journal of Mechanical Precision Engineering

Journal homepage:
<https://semarakilmu.my/index.php/sijmpe/index>
ISSN: 3083-9564



Finite Element Analysis and Response Surface Optimization for Structure of Dry Ice Cleaning Machine Frame

Ma Haohao^{1,2}, Mohd Zuhri Mohamed Yusoff^{1,3,*}, Azizan As'array¹, Adi Azriff Basri⁴, Muhammad Shahril Shahbudin⁵, Ezzat Afifi Abd Halid⁵, Muhammad Safwan Abdul Aziz⁵

¹ Department of Mechanical and Manufacturing Engineering, Faculty of Engineering, Universiti Putra Malaysia, 43400, Serdang, Selangor, Malaysia

² Department of Mechanical Engineering, School of Mechatronics and Automotive Engineering, Tianshui Normal University, 741001, Tianshui, China

³ Laboratory of Biocomposite Technology, Institute of Tropical Forestry and Forest Products (INTROP), Universiti Putra Malaysia, 43400, UPM Serdang, Selangor, Malaysia

⁴ Department of Aerospace Engineering, Faculty of Engineering, Universiti Putra Malaysia, 43400, Serdang, Selangor, Malaysia

⁵ AIIS Solutions Sdn Bhd, No. 12, Jalan Tiara Sentral 1, Nilai Utama, Enterprise Park, 71800, Nilai, Negeri Sembilan, Malaysia

ARTICLE INFO

Article history:

Received 14 December 2024

Received in revised form 12 January 2025

Accepted 28 February 2025

Available online 15 March 2025

Keywords:

Dry ice cleaning; finite element analysis; Response Surface Optimization; modal analysis

ABSTRACT

This study aims to optimize the design of a dry ice cleaning machine frame. According to the typical working condition data of the dry ice cleaning machine, the Finite Element Analysis (FEA) was used for static structural analysis. It is found that the U-shaped tube is the most easily damaged component. The Response Surface Optimization (RSO) method was used in this study to optimize the parameters of the U-shaped tube size. Here, the maximum total deformation is reduced from 0.058 to 0.022 mm compared to the original design, and the mass is increased by 2.43 kg. Subsequently, the modal analysis of the optimized dry ice cleaning machine frame was carried out to determine the first 6 natural frequencies and vibration modes. The results show that the optimization design of the dry ice cleaning machine frame effectively improves the working reliability of key components, and the overall frame is also in a safe state. This study provides theoretical and practical guidance for the design and improvement of dry ice cleaning machines.

1. Introduction

As the main bearing mechanism of the working parts of the dry ice cleaning machine, the frame plays a role in supporting and protecting the working parts. It must have sufficient strength and rigidity to bear its weight and various workloads. Studying the strength of the rack is of great significance to improving the safety of the dry ice cleaning. Among related research results, Zhang *et al.*, [1] took the parallel manipulator as the research object, introduced its load setting, calculation method of strength and stiffness, simplification of frame model and finite element analysis method,

* Corresponding author.

E-mail address: zuhri@upm.edu.my

<https://doi.org/10.37934/sijmpe.2.1.1123a>

and combined with its actual working conditions, it carried out finite element force analysis and passed the strength test. Premanand *et al.*, [2] conducted modal analysis on the frame to obtain the natural frequency and mode shape of the frame, thus providing a basis for the structural dynamics design. Yusufoglu *et al.*, [3] obtained the frame modal analysis resonant frequency, topological analysis and structural improvement of the frame, successfully solved the problem of frame resonance.

Many researchers have used computational methods to study the structural design and optimization of equipment racks in the industrial field. Using Finite Element Analysis (FEA) to analyze mechanical equipment is as important as physical experiments.[4] The research process can help designers evaluate the performance of the structure under various working conditions, reduce the capital investment of experiments, and improve efficiency [5,6]. Current research is mainly focused on static analysis, dynamic analysis, modal analysis, and structural parameter optimization [7]. FEA can simulate and calculate the component structure's stress distribution, deformation, strain energy, and failure points. Compared with physical experimental measurement methods, this method significantly improves the accuracy of structural evaluation [8,9]. It effectively solves the possibility of ignoring local factors caused by simplifying theoretical calculation problems [10].

The application of FEA in the frame structure design of equipment is used to optimize the stiffness-to-weight ratio, which can reduce the amount of material used while maintaining the strength of the machine [11]. FEA has enhanced dynamic stability and vibration resistance in mechanical automation systems to ensure high-speed operation accuracy [12]. Similarly, in heavy cleaning equipment (including dry ice cleaning machines), FEA helps to identify potential failure areas, optimize component geometry, and predict long-term durability under operating loads [13]. These studies highlight the importance of structural analysis in improving machine performance, but limited research has been conducted on dry ice blasting racks [14].

Despite advances in structural optimization, challenges remain in improving the mechanical performance of dry ice blasting racks. Conventional rack designs often prioritize material savings over performance, leading to localized stress concentrations, excessive deformation, and possible structural failure under operating loads [15]. Additionally, vibration-induced resonances pose significant risks that can compromise the efficiency and life of the machine [16]. This study takes the frame of dry ice cleaning to establish a three-dimensional model of the frame and uses ANSYS Workbench to conduct finite element analysis on it. By analyzing the force characteristics under typical working conditions, and applying constraints and loads under various working conditions, the displacement and stress contours of the frame are obtained.

The specific objectives of this study are:

- i) Develop a 3D finite element model of the frame using ANSYS Workbench.
- ii) Static structural analysis to evaluate stress distribution and deformation under typical operating conditions.
- iii) Apply response surface optimization (RSO) techniques to reduce frame deformation while maintaining structural integrity.
- iv) Perform modal analysis to determine natural frequencies and vibration modes to ensure that the frame design minimizes the risk of resonance.

Section 2 of this paper presents the methodology in detail, including the development of the finite element model, static structural analysis methods, and response surface optimization strategies. Section 3 presents the results and discussion, covering the main findings from the finite element simulations, optimization, and modal analysis results. Section 4 concludes the study,

summarizes the main contributions, discusses potential engineering applications, and suggests directions for future research in structural optimization and airframe design.

2. Methodology

The workflow of optimizing the structural design of the dry ice cleaning machine frame in this study is shown in Figure 1. The method includes finite element modeling of the dry ice cleaning machine, static structural analysis, response surface optimization, and modal analysis.

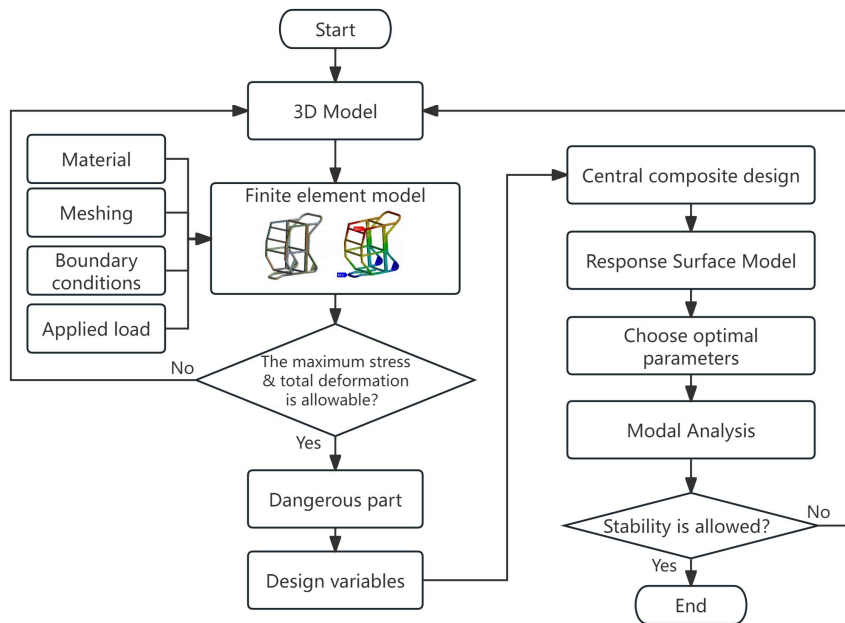


Fig. 1. Flowchart of the research methodology

After establishing the 3D model of the frame, the FEA model is established by combining material properties, meshing, boundary conditions, and applied loads. The stress distribution and total deformation under working conditions are evaluated by FEA, and the most vulnerable structural components are determined. To further optimize the structure of the dry ice cleaning machine, the RSO method is applied, and the central composite design is used to determine the optimal design parameters. The stability of the optimized model is verified by modal analysis to ensure that the natural frequencies and vibration modes of the frame do not cause resonance and impair the stability of the machine.

2.1 Frame Statics Analysis Theory

Static analysis applies different constraints and static loads to the analysis object according to each working condition and calculates the maximum displacement and maximum stress of the frame through the basic formula of static analysis. By comparing the yield strength of the material, it is determined whether it meets safety. The basic formula of static analysis is shown in Eq. (1).

$$[K]\{\delta\} = [F] \quad (1)$$

In the Eq. (1), $[K]$ represents the overall stiffness matrix of the model; $\{\delta\}$ represents the overall displacement matrix of the model; $[F]$ represents the overall load matrix of the model [17].

The fourth strength theory is used to judge whether the structure fails. The fourth strength theory is shown in Eq. (2).

$$\sigma_{eq} = \sqrt{\frac{1}{2}[(\sigma_1 - \sigma_2)^2(\sigma_2 - \sigma_3)^2(\sigma_3 - \sigma_1)^2]} < [\sigma] \quad (2)$$

In Eq. (2), σ_{eq} represents the Von Mises stress; $\sigma_1, \sigma_2, \sigma_3$ represent the first principal stress, the second principal stress, and the third principal stress; $[\sigma]$ represents the allowable stress of the material, that is, the yield stress.

2.2 Frame Modal Analysis Theory

As a multi degree of freedom structure, the vibration characteristics of the frame can be calculated by the finite element method and linear vibration theory. Based on the principle of virtual work, establish the motion equation of the vehicle frame as shown in Eq. (3).

$$[M]\{\ddot{\delta}\} + [C]\{\dot{\delta}\} + [K]\{\delta\} = \{F\} \quad (3)$$

In Eq. (3), $[M]$ represents the quality matrix; $[C]$ represents the damping matrix; $[K]$ represents the stiffness matrix; $\{F\}$ represents the load matrix; $\{\delta\}$ represents the displacement matrix [18].

In modal analysis, $\{F\}=0$ is taken because external loads are ignored; At the same time, the structural damping is very small and can be ignored. Eq. (3) can be simplified to Eq. (4).

$$[M]\{\ddot{\delta}\} + [K]\{\delta\} = 0 \quad (4)$$

The solution of the differential equation in Eq. (4) is by using Eq. (5).

$$\{\delta\} = \{\delta_0\} \sin(\omega t + \varphi) \quad (5)$$

In Eq. (5), $\{\delta_0\}$ represents the amplitude column vector; ω represents the natural frequency of vibration; φ represents the initial phase of the vibration. Substitute Eq. (5) into Eq. (4) to obtain Eq. (6).

$$([K] - \omega^2[M])\{\delta_0\} = 0 \quad (6)$$

The necessary and sufficient condition for Eq. (6) to have a non-zero solution is Eq. (7).

$$[K] - \omega^2[M] = 0 \quad (7)$$

By solving Eq. (7), its eigenvalues and corresponding eigenvectors, namely the n -th natural frequency and main mode of the system, can be obtained.

3. Results

3.1 Frame Structure

This frame is composed of multiple complex longitudinal beams and multiple crossbeams, and is a typical side beam structural frame, as shown in Figure 2. The basic parameters of the frame and the distance between each crossbeam are measured, with a length of approximately 868 millimeters, a width of 468 millimeters, and a height of 1000 millimeters. To ensure the accuracy of the analysis results, when geometric modeling the framework, a three-dimensional model of the framework is established at a 1:1 ratio.

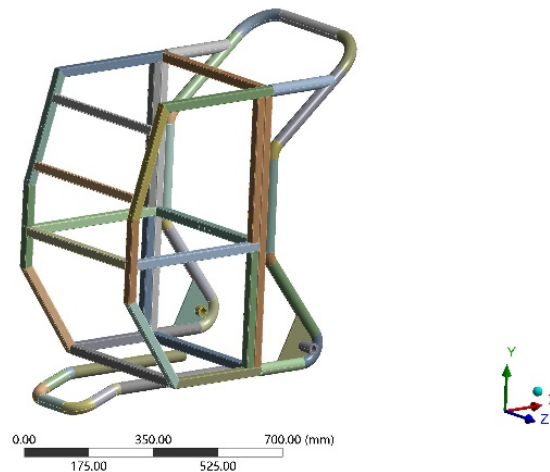


Fig. 2. Frame structure diagram and parameters

3.2 Build the Frame Finite Element Model

The frame is made of stainless steel, which is an alloy steel composed primarily of iron, with a minimum of 10.5% chromium content. This chromium content forms a protective chromium oxide layer on the surface, which provides excellent corrosion resistance. The physical performance parameters of its materials are shown in Table 1.

Table 1
Relevant parameters of stainless-steel material

Name	parameter
Density/(kg/m ³)	7750
Young's modulus/GPa	193
Poisson's ratio	0.31
Tensile strength/MPa	207
Bulk Modulus/GPa	169.3
Shear Modulus/GPa	73.664

A solid element tetrahedral and hexahedral types have been selected to mesh the frame model. The unit is defined by 25 movable bodies. Use a hexahedral mesh for the tubes. Tetrahedral meshing flexibly adapts to complex geometries and irregular shapes, ensuring accurate representation of complex structures. This meshing method provides fine control over mesh density, efficiently allocating computational resources by concentrating mesh elements in regions of interest while maintaining a coarser mesh elsewhere to reduce computational overhead.

The mesh uses an element size of 0.05 mm, with a total number of nodes around 141916, and the number of elements is 68671. The mesh diagram of the division is shown in Figure 3.

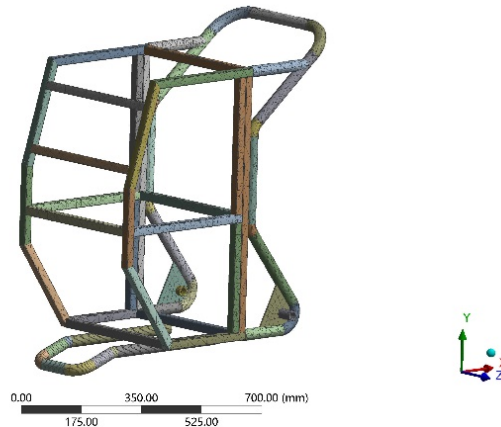


Fig. 3. Mesh model of frame

3.3 Static Structure Analysis of Frame

This study analyzes the ultimate force and deformation of the frame under various working conditions. The loads on the frame mainly include; the weight of the dry ice cleaning, the weight of the dry ice, the weight of the packing box, and the weight of some other accessories. The weight of the frame is 18 kg, the weight of the mechanical equipment it carries is 35 kg, and up to 2 kg of dry ice can be added during operation.

For the convenience of describing the constraint conditions in the following text, the coordinate system of the frame model is agreed as follows; the X-direction represents the lateral direction of the frame, the Y-direction represents the longitudinal direction of the frame, and the Z-direction represents the vertical direction of the frame. On the basis of the above, a static structural analysis was conducted to obtain the displacement and stress cloud picture of the frame under full load bending conditions, as shown in Figures 4 and 5, respectively.

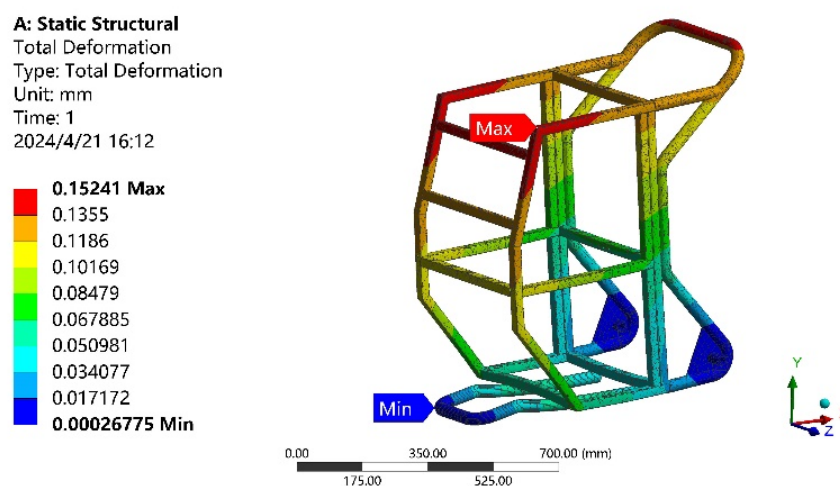


Fig. 4. Cloud picture of displacement

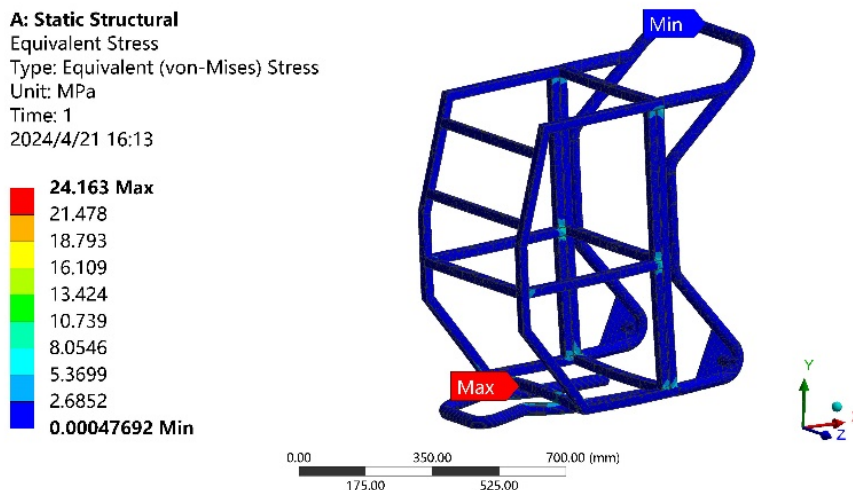


Fig. 5. Cloud picture of stress

As shown in Figure 4, the maximum displacement of the frame is approximately 0.15 mm, mainly due to the large mass of equipment carried by the upper crossbeam of the frame. Compared to the overall size of the frame, the deformation is very small and can be ignored, indicating that the stiffness of the frame meets the requirements.

Figure 5 shows that the maximum equivalent stress on the frame is 24.16 MPa, and there is stress concentration here. Then further analyze the total structural deformation and equivalent stress of the structure involved here. The total deformation of the bottom U-shaped tube under stress is shown in Figure 6, which shows that this structure is the most dangerous position compared with other structures.

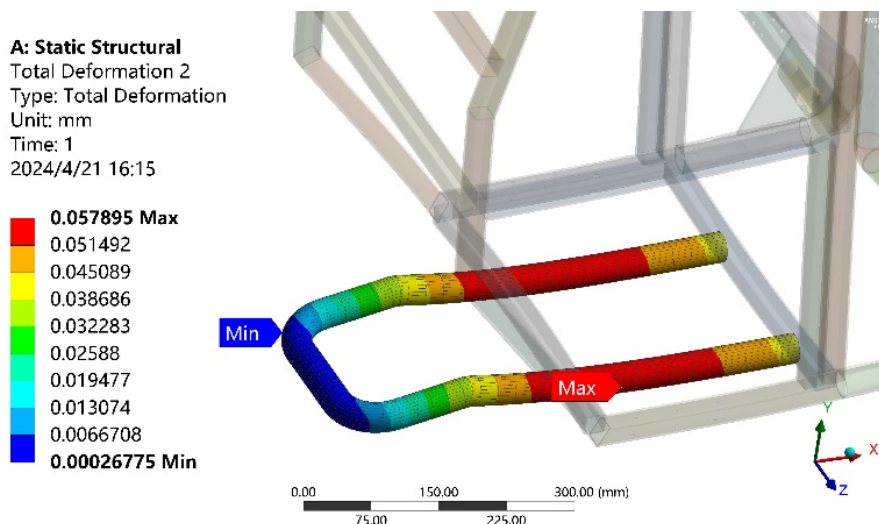


Fig. 6. Total deformation of U-shaped tube

3.4 Parametric Modeling

Response surface optimization is a statistical technique used to optimize complex processes or systems by constructing and analyzing mathematical models of the relationship between input variables and output responses. In response surface optimization, a series of experiments are conducted to collect data on the system's responses under different input conditions. These data are

then used to fit a mathematical model. Once the model is constructed, optimization algorithms are employed to identify the input variable settings that lead to optimal or desired responses.

The inner diameter $r_i = 14$ mm and the outer diameter $r_o = 17$ mm in the current design plan. The U-shaped tube has a symmetrical structure, so the stressed beam element is selected as the analysis object and the same load effect is applied. Figure 7 is a cloud diagram of the unilateral force deformation of the U-shaped tube. Its maximum deformation is 0.058 mm, which matches Figure 6.

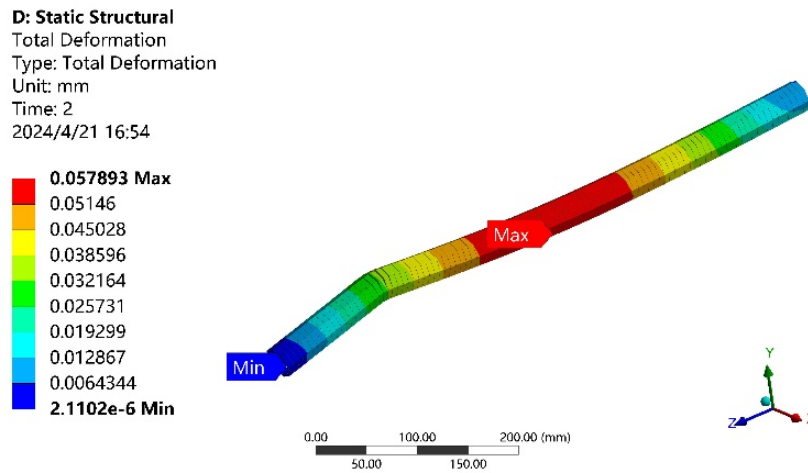


Fig. 7. Unilateral deformation of U-shaped tube

In this design, the U-shaped pipe with the largest deformation is designed parametrically. The inner diameter and outer diameter of the pipe are used as design variables to solve for the minimum mass and minimum total deformation, as shown in Eq. (8).

$$\left\{ \begin{array}{l} X = [r_i, r_o] \\ \min f(X) = a \cdot \text{Mass} + b \cdot \text{Deformation} \\ \text{Subject to } \begin{cases} r_{i_{\min}} \leq r_i \leq r_{i_{\max}} \\ r_{o_{\min}} \leq r_o \leq r_{o_{\max}} \end{cases} \end{array} \right. \quad (8)$$

3.5 Design of Experiments

This experimental design uses a Central Composite Design (CCD), which enhances the traditional factorial design by adding center points and pivot points to more effectively evaluate the impact of input variables on system response. CCD includes three types of design points: center point, axial point, and orthogonal point. By conducting experiments based on the CCD method, mathematical models can be developed that relate system responses to input variables, allowing for optimization and prediction. Design Points of Design of Experiments are shown in Table 2, the variation interval of parameter r_i is (10, 15), and the interval of r_o is (15.5, 20).

Table 2
 Design Points of Design of Experiments

Name	ri (mm)	ro (mm)	Mass(kg)	Deformation(mm)
1	12.5	17.75	2.55	0.035
2	10	17.75	3.45	0.029
3	15	17.75	1.45	0.054
4	12.5	15.5	1.35	0.078
5	12.5	20	3.91	0.019
6	10	15.5	2.25	0.054
7	15	15.5	0.24	0.368
8	10	20	4.82	0.017
9	15	20	2.81	0.024

With experiments specified in the CCD design, the fitted mathematical model can be visualized through response surface plots. The response surface of r_i and r_o to the total deformation is shown in Figure 8, and the response surface of r_i and r_o to the mass is shown in Figure 9. Response surface plots provide a graphical representation of system behavior and help improve r_i and r_o decision-making.

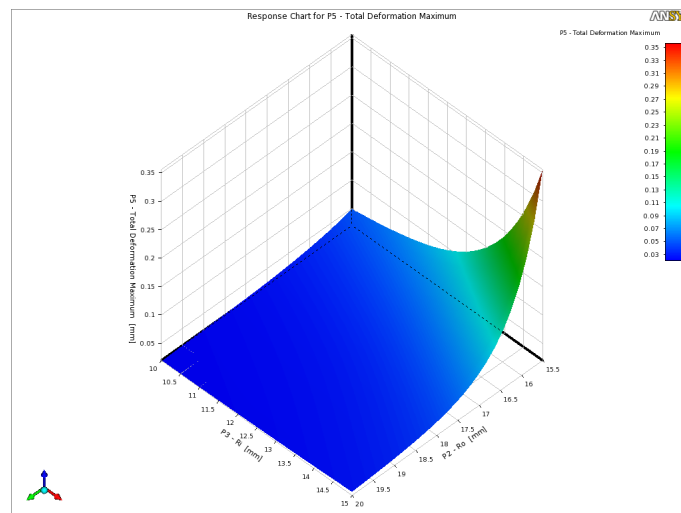


Fig. 8. Response surface of r_i and r_o to Deformation

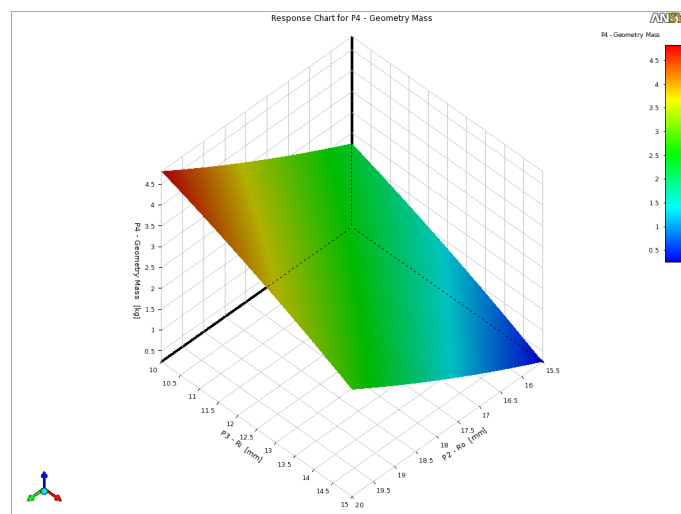


Fig. 9. Response surface of r_i and r_o to Mass

After constructing the response surface model of the relationship between the inner diameter, outer diameter, and mass and deformation, 1000 sets of sampling points were generated, as shown in Figure 10. These sampling points represent various combinations of inside and outside diameters. Based on predefined criteria or targets, the best solution for the inner and outer diameters is selected from this set of sample points, as shown in Figure 11.

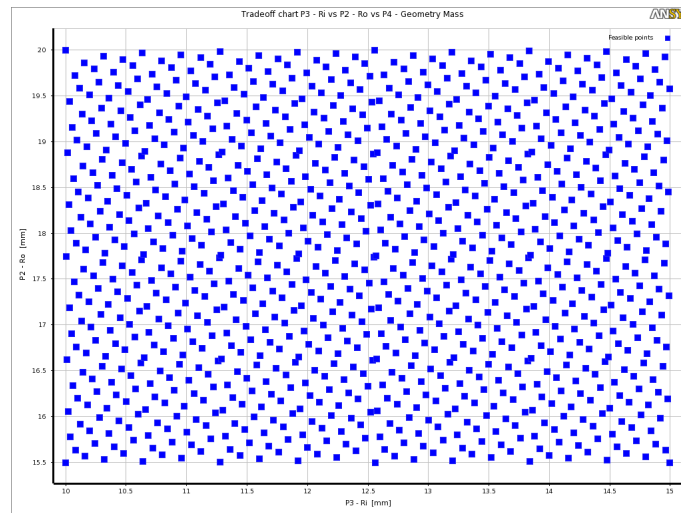


Fig. 10. 1000 sets of sampling points

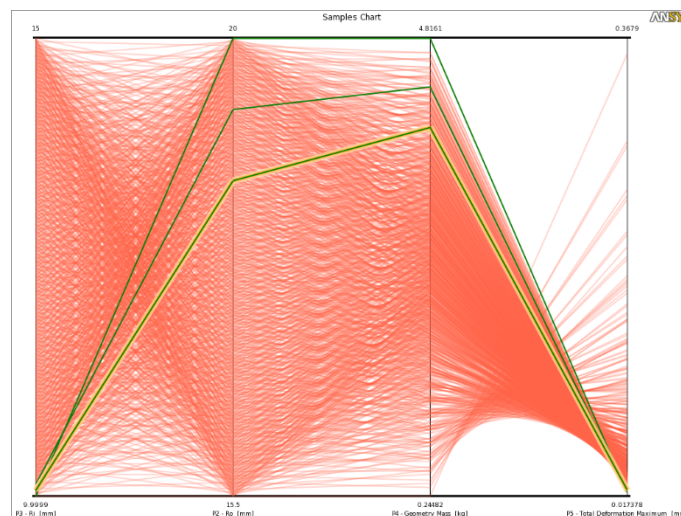


Fig. 11. The best solution of sampling points

The comparison of the optimized scheme and the original results is shown in Table 3. It can be seen that the total deformation is reduced from the original 0.058 to 0.022 mm, that is, the total deformation is reduced by 61.71%. Of course, the mass has increased by 2.43 kg. This design can select similar stainless steel 304 according to the model of the stainless-steel profile.

Table 3

Optimized design parameters compared with original parameters

Name	ri (mm)	ro (mm)	Mass (kg)	Deformation (mm)
Original	14	17	1.493	0.057893
Optimized	10.068	18.596	3.9244	0.022166

3.6 Frame Modal Analysis Results

The natural frequency and vibration mode are the inherent characteristics of the frame structure. The constraint conditions applied in modal analysis are as follows: the right front wheel constrains the translational degrees of freedom in the X, Y, and Z directions, the left front wheel constrains the translational degrees of freedom in the Y and Z directions, and the truss only constrains the translational degrees of freedom in the Z direction.

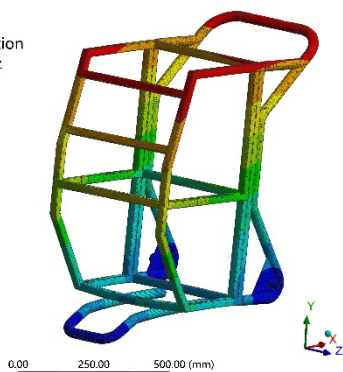
The Block Lanczos calculation method was used to obtain the first six natural frequencies and vibration modes of the orchard operation machinery frame, as shown in Table 4 and Figure 12, respectively.

Table 4
 Modal Analysis Results of Vehicle Frame

Modal order	Natural frequency/Hz	Vibration mode description
1	40.47	Longitudinal swing of rear support beam
2	41.83	Lateral swing of rear support beam
3	87.41	Middle vertical swing
4	135.62	Longitudinal torsion of rear support beam
5	145.33	Middle support beam lateral swing
6	168.95	Longitudinal swing of the middle support beam

F: Modal
 Total Deformation 1
 Type: Total Deformation
 Frequency: 40.466 Hz
 Unit: mm
 2024/4/22 11:54

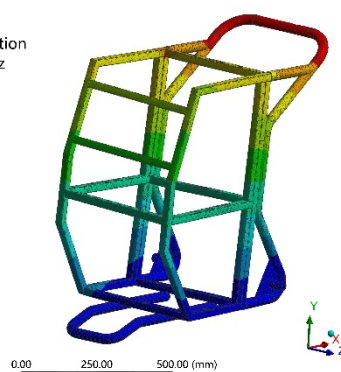
10.466 Max
 9.3044
 8.1424
 6.9805
 5.8185
 4.6565
 3.4945
 2.3325
 1.1706
 0.0085831 Min



(a)

F: Modal
 Total Deformation 2
 Type: Total Deformation
 Frequency: 41.826 Hz
 Unit: mm
 2024/4/22 11:54

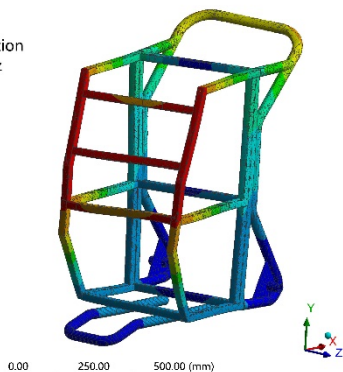
12.347 Max
 10.976
 9.6042
 8.2328
 6.8614
 5.49
 4.1186
 2.7472
 1.3757
 0.0043233 Min



(b)

F: Modal
 Total Deformation 3
 Type: Total Deformation
 Frequency: 87.405 Hz
 Unit: mm
 2024/4/22 11:54

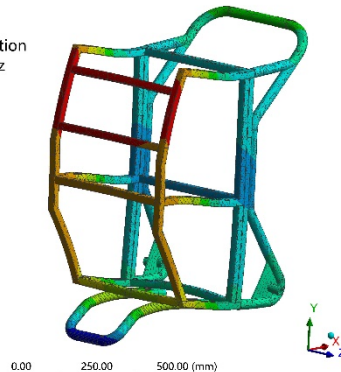
13.11 Max
 11.654
 10.198
 8.7412
 7.2848
 5.8285
 4.3721
 2.9158
 1.4594
 0.0030652 Min



(c)

F: Modal
 Total Deformation 4
 Type: Total Deformation
 Frequency: 135.62 Hz
 Unit: mm
 2024/4/22 11:54

12.256 Max
 10.902
 9.5472
 8.1928
 6.8384
 5.4841
 4.1297
 2.7753
 1.421
 0.066589 Min



(d)

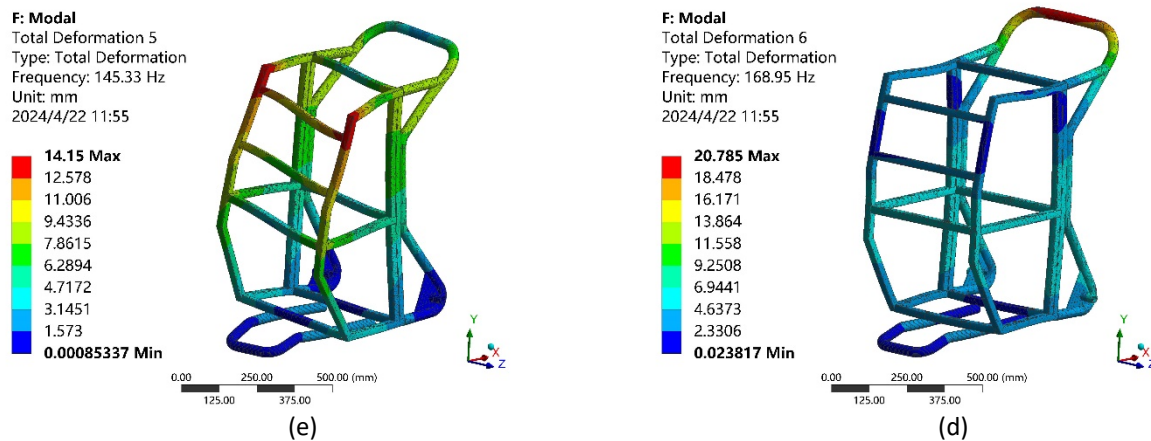


Fig. 12. The first six-order natural modes of the frame, where (a) 1st order, (b) 2nd order, (c) 3rd order, (d) 4th order, (e) 5th order and (f) 6th order mode shapes

From Figure 12, it can be seen that the first mode of vibration is the longitudinal oscillation of the rear support beam, and the deformation of the frame is mainly concentrated in the rear support beam, with a deformation amount of 10.47 mm; The second mode of vibration is the lateral oscillation of the rear support beam, with a deformation of 12.44 mm; The third mode of vibration is the central vertical oscillation, with a deformation of 13.11 mm; The fourth mode of vibration is the longitudinal torsion of the rear support beam, with a deformation of 12.26 mm; The fifth mode of vibration is the lateral oscillation of the middle support beam, with a deformation of 14.15 mm; The sixth mode of vibration is the longitudinal oscillation of the middle support beam, with a deformation of 20.79 mm.

4. Conclusions

In this study, a static structure analysis was conducted on the frame. Based on the operational characteristics of the dry ice cleaning, a full-load working condition was selected for analysis to obtain the maximum displacement cloud picture and stress cloud picture results. Comparing the analysis results with the actual material properties of the frame, it was found that the U-shaped tube structure at the bottom of the frame is the most dangerous location. Therefore, the response surface optimization method was used to optimize the size of the U-shaped tube structure. The maximum total deformation is reduced from 0.058 to 0.022 mm compared with the original design, and the mass is increased by 2.43 kg. Finally, a modal analysis was performed on the optimized frame, and the first six natural frequencies and natural vibration modes of the frame were obtained. During the design process of the frame, the natural frequencies of the frame should avoid external excitation. If this is not possible, vibration damping can be installed on the frame to avoid resonance.

Acknowledgement

The authors would like to thank Universiti Putra Malaysia for continuous support of the research work. The contributions of Mr. Muhammad Faris Idrus in the successful implementation of this project are very much appreciated.

References

- [1] Zhang, Shuangshuang, and Linsong Zhang. "Stiffness Modeling and Deformation Analysis of Parallel Manipulators Based on the Principal Axes Decomposition of Compliance Matrices." *Journal of Mechanisms and Robotics* 16, no. 4 (2023). <https://doi.org/10.1115/1.4062134>

- [2] Premanand, Aravind, and Frank Balle. "Stress and Strain Calculation Method for Orthotropic Polymer Composites under Axial and Bending Ultrasonic Fatigue Loads." *Ultrasonics* 135 (2023/12/01/ 2023): 107130. <https://doi.org/https://doi.org/10.1016/j.ultras.2023.107130>
- [3] Ince Yusufoglu, S., E. Saricam, and M. S. Ozdogan. "Finite Element Analysis of Stress Distribution in Root Canals When Using a Variety of Post Systems Instrumented with Different Rotary Systems." [In eng]. *Ann Biomed Eng* 51, no. 7 (Jul 2023): 1436-48. <https://doi.org/10.1007/s10439-023-03145-w>
- [4] Srivastava, Shekhar, Rajiv Kumar Garg, Sachdeva Anish, Vishal Sharma, Singh Sehijpal, and Munish Gupta. "Distribution of Temperature and Residual Stresses in Gma-Ded Based Wire-Arc Additive Manufacturing." *Rapid Prototyping Journal* 29 (07/31 2023). <https://doi.org/10.1108/RPJ-01-2023-0032>
- [5] Patel, Vilas, Sareen Duseja, and Dhaval Jivani. "Effect of Different Implant Internal Crest Module Designs on Abutment Stability and Screw Passivity: A Finite Element Analysis." *International Journal of Prosthodontics and Restorative Dentistry* 12 (05/03 2023): 185-90. <https://doi.org/10.5005/jp-journals-10019-1390>
- [6] Haohao, M., A. As'arry, F. Yanwei, C. Lulu, A. Delgoshaei, M. I. S. Ismail, and H. R. Ramli. "Improved Black-Winged Kite Algorithm and Finite Element Analysis for Robot Parallel Gripper Design." Article. *Advances in Mechanical Engineering* 16, no. 10 (2024). <https://doi.org/10.1177/16878132241288402>
- [7] Asif, Aayisha, Megha Dhanapal, U. S. Megha, Siniya Nazar, and Sherry Rose Jose. "Analysis of Steel–Concrete Composite Beam Using Ansys 18.1 Workbench." *Materials Today: Proceedings* (2023). <https://doi.org/10.1016/j.matpr.2023.05.285>
- [8] Chourasia, Kajal, and Sharnappa Joladarashi. "Modelling, Static and Dynamic Analysis of Offset Bearing Using Ansys." *Materials Today: Proceedings* 66 (2022): 2124-32. <https://doi.org/10.1016/j.matpr.2022.05.560>
- [9] Chakravarthy, C. H. Nithin, S. Sathees Kumar, and K. Tirupathi. "Comparison and Identification of Fracture Behaviors of an Alloy Material through Ansys." *Materials Today: Proceedings* 46 (2021): 944-55. <https://doi.org/10.1016/j.matpr.2021.01.186>
- [10] Mali, Rohit, and Uday Pise. "Modeling Elastic Properties of Biocomposites Using Various Analytical Models and Ansys Material Designer." *Materials Today: Proceedings* 72 (2023): 1372-78. <https://doi.org/10.1016/j.matpr.2022.09.334>
- [11] Rayhan, Saiaf Bin, and Md Mazedur Rahman. "Modeling Elastic Properties of Unidirectional Composite Materials Using Ansys Material Designer." *Procedia Structural Integrity* 28 (2020): 1892-900. <https://doi.org/10.1016/j.prostr.2020.11.012>
- [12] Kalapodis, Nicos A., Edmond V. Muho, and Dimitri E. Beskos. "Structure-Specific, Multi-Modal and Multi-Level Scalar Intensity Measures for Steel Plane Frames." *Soil Dynamics and Earthquake Engineering* 190 (2025): 109185. <https://doi.org/10.1016/j.soildyn.2024.109185>
- [13] Liu, Hongbo, Wenqiang Zhang, Huiyun Chen, and Zhihua Chen. "Damage Analysis and Mechanical Performance Evaluation of Frame Structures in Recycling." *Structures* 66 (2024): 106906. <https://doi.org/10.1016/j.istruc.2024.106906>
- [14] Lian, Ming, Binlin Guan, Qianqian Cheng, Hao Zhang, and Mingzhou Su. "Experimental and Numerical Study of Seismic Performance of High-Strength Steel Fabricated Framed-Tube Structures with Replaceable Shear Links." *Structures* 28 (2020): 2714-32. <https://doi.org/10.1016/j.istruc.2020.10.081>
- [15] Montuori, Rosario, Elide Nastri, Vincenzo Piluso, and Alessandro Pisapia. "Design Procedure for Failure Mode Control of Linked Column Frames." *Engineering Structures* 296 (2023): 116937. <https://doi.org/10.1016/j.engstruct.2023.116937>
- [16] Agrawal, Anant Prakash, Shahazad Ali, and Sachin Rathore. "Finite Element Stress Analysis for Shape Optimization of Spur Gear Using Ansys." *Materials Today: Proceedings* 64 (2022): 1147-52. <https://doi.org/10.1016/j.matpr.2022.03.404>
- [17] Qi, Taining, Tao Yan, Shiju Song, Yu Zhu, and Geng Chen. "Topology Optimization of a Ratchet Compensation Structure Subject to Periodic Constraints." *High-speed Railway* 2, no. 4 (2024): 230-40. <https://doi.org/10.1016/j.hspr.2024.11.003>
- [18] Yang, Han, Ninghao Liu, Mengjie Gu, Qiang Gao, and Zhipeng Jiao. "Multi-Objective Parameter Optimization of U-Type Air-Cooled Thermal Management System Based on a Surrogate Model." *International Journal of Thermal Sciences* 212 (2025): 109707. <https://doi.org/10.1016/j.ijthermalsci.2025.109707>